SUPPLEMENTARY INFORMATION

Supplementary Tables

Supplementary Table I – Compositions of INNER and OUTER PM simulations.

(A) OUTER

lipid	structure	number
PSM	SM 34:1;2	81
PLPC	PC 16:0;0-18:2;0	99
NSM	SM 42:2;2	63
LSM	SM 42:1;2	54
SOPC	PC 18:0-18:1	45
PAPC	PC 16:0-20:4	36
SAPS	PS 18:0-20:4	9
PLAS	PE-O 18:1-20:4	18
CHOL	cholesterol	270

(B) INNER

lipid	structure	number
PAPS	PS 16:0-20:4	90
PLPC	PC 16:0-18:2	63
POPC	PC 16:0-18:1	27
PLQS	PE-O 18:1-22:4	63
POPE	PE 16:0-18:1	18
PDPE	PE 16:0-22:6	54
OAPE	PE 18:1-20:4	27
PLAO	PE-O 18:2-20:4	18
DPPC	PC 16:0-16:0	18
PSM	SM 34:1;2	9
OAPS	PS 18:0-20:4	9
PIP2	PIP2 18:1-20:4	18
CHOL	cholesterol	279

Supplementary Table II – Compiled inner and outer leaflet lipidomes of RBCs

(A) Outer leaflet compiled lipidome

Category	Notes	representative lipid	mol% of outside phospholipids	scaled to 100%
1	a,b	PC 16:0-18:2	19.7	22.2
2	a	SM 34:1;2	19.8	22.4
3		SM 42:2;2	16.4	18.5
4	c	SM 42:1;2	12.8	14.4
6	e	PC 16:0-20:4	8.6	9.7
5		PC 18:0-18:1	7.5	8.4
9	d	PC 18:1-18:2	1.8	2.0
7	e	PS 18:0-20:4	1.3	1.5
8	e	PI 18:0-22:4	0.8	0.9

(B) Inner leaflet compiled lipidome

category	notes	representative lipid	mol% of inner phospholipds	scaled to 100%
1	a,e	PS 16:0-20:4	25.9	33.1
2	f,a	PE O- 18:1-22:4	10.7	13.7
3	a	PC 16:0-18:2	10.2	13.0
4	a, i	PE 16:0-22:6	9.3	11.9
5	h	PE 18:1-20:4	5.4	6.9
6		PC 16:0-18:1	5.5	7.0
7		PE 16:0-18:1	3.7	4.8
8	g	PE O- 18:2-20:4	2.9	3.7
9	a	PC 16:0-16:0	2.3	2.9
11		SM 34:1;2	1.5	2.0
10		PI 18:0-20:4	0.8	1.0

a	Generally, combining lipids differing by 2 carbons and naming them by the more abundant one (eg SM 34:1 is PSM and represents this species and SM 36:1)
c	SMs usually have a trans double bond in the long-chain base. This is not counted as an unsaturation. This class includes SMs with an unsaturated acyl chain, including both 24:2 and shorter unsaturated species like SM 36:2
d	includes all PC species with two unsaturated acyl chains
e	includes lipids with the designed headgroup and one highly polyunsaturated acyl chain like 20:4 or 22:6
f	For most ether lipids, there is a double bond in the vinyl ether connecting the backbone to the sn-1 hydrophobic chain. This double bond is not counted as an acyl chain unsaturation per se. Thus, this class is separate from the class which includes the more typical w-9 unsaturated acyl chains in the sn-1 (eg PE-O 18:2/20:4)
g	plasmalogen with C18:1 in the SN1
h	includes all PE with both acyl chains unsaturated
i	includes all PE containing one saturated acyl chain and one with 2 or more unsaturations

Supplementary Figures

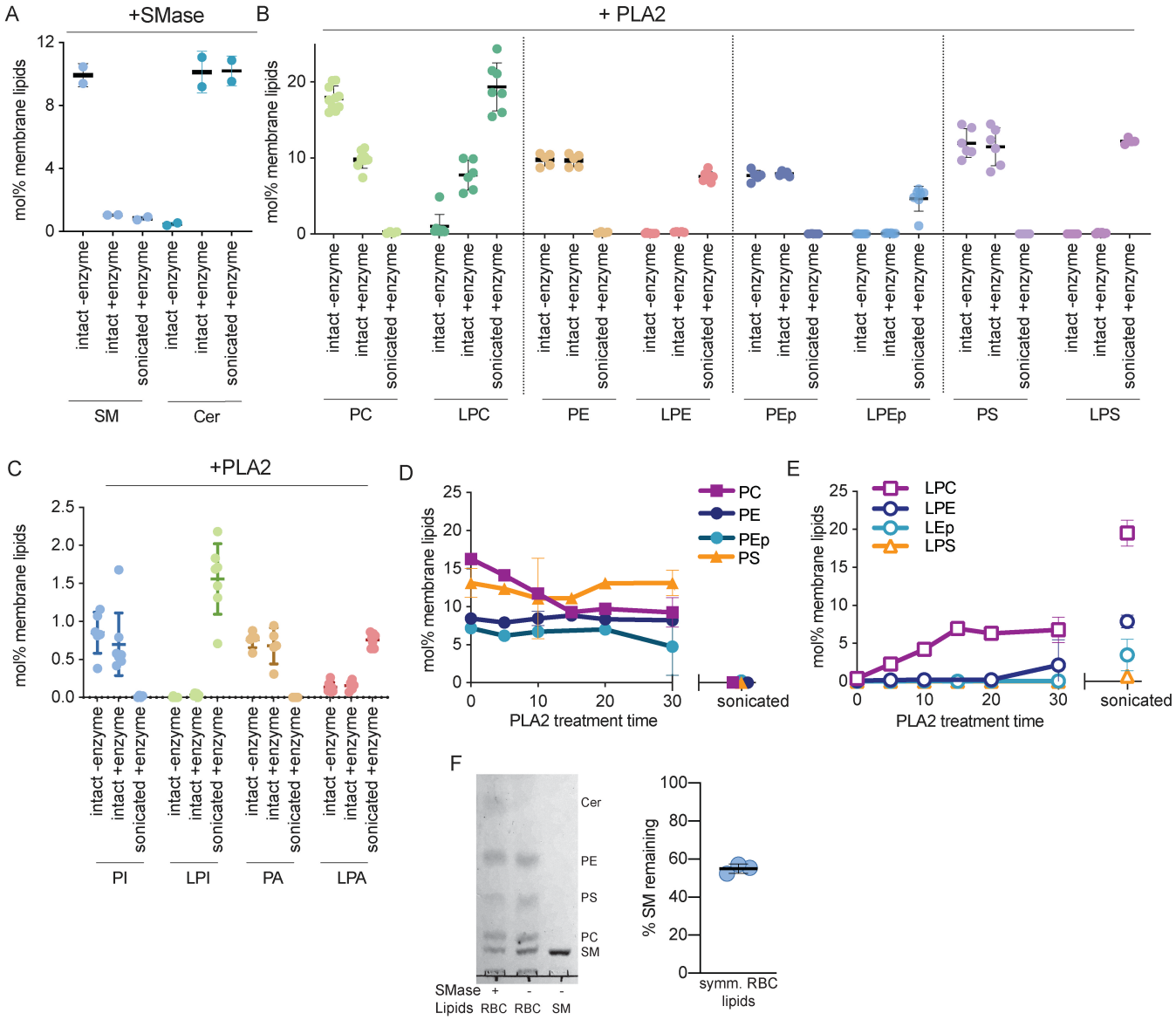

Supplementary Figure 1 – Lipidomics of enzyme treated erythrocytes (RBCs). (A) SMase treatment of intact RBCs degraded ~90% of SM. Treatment of sonicated cells degraded essentially all SM, confirming enzyme potency. Notably, Cer (the product of the SMase reaction) was produced in quantitative agreement with the consumption of SM. Because SM and Cer are quantified using distinct internal standards, the excellent agreement between product generation and reactant consumption confirms quantitative accuracy of the lipidomic measurements. (B-C) Lipidomics after PLA2 treatment of intact and sonicated RBCs. PLA2 did not degrade measurable amounts of PS, PE, PE O-, PI, or PA in intact cells, but completely degraded those in cells disrupted by sonication. These results suggest that such lipids are exclusively on the inner PM leaflet. Again, the quantitative agreement between phospholipids consumed by the reaction and lysolipids generated supports the accuracy of the measurements. (D) Lipid hydrolysis by PLA2 time course. Progressive degradation of PC produces progressive generation of (E) LPC. The reaction saturates at 15 minutes, suggesting all accessible phospholipids are degraded. All other enzyme treatments were done for 30 min. (F) Lipids were extracted from RBCs and reconstituted into 100 nm liposomes. These liposomes were then treated with SMase and the results analyzed via thin layer chromatography (SM lipid standard in rightmost lane). The intensity of the SM band was reduced by enzymatic treatment (left lane). This effect was quantified by densitometry, normalizing to PC, PE, and PS in the same sample. SM was reduced by ~50% by treatment of the symmetric liposomes with SMase, as would be expected from near-complete digestion of all outer leaflet SM. (A-C) Each data point represents results from a single RBC isolation and treatment. Mean ± SD are shown. (D) Mean ± SD are shown, from 3 independent experiments. (F) Each data point represents results from a single experiment. Mean ± SD are shown. In total, three different donors were used, some for multiple isolations. As there were no notable differences between donors or isolation days, all samples were combined. Supplementary Figure 2 shows the variance between the individual experimental measurements for all PC species.

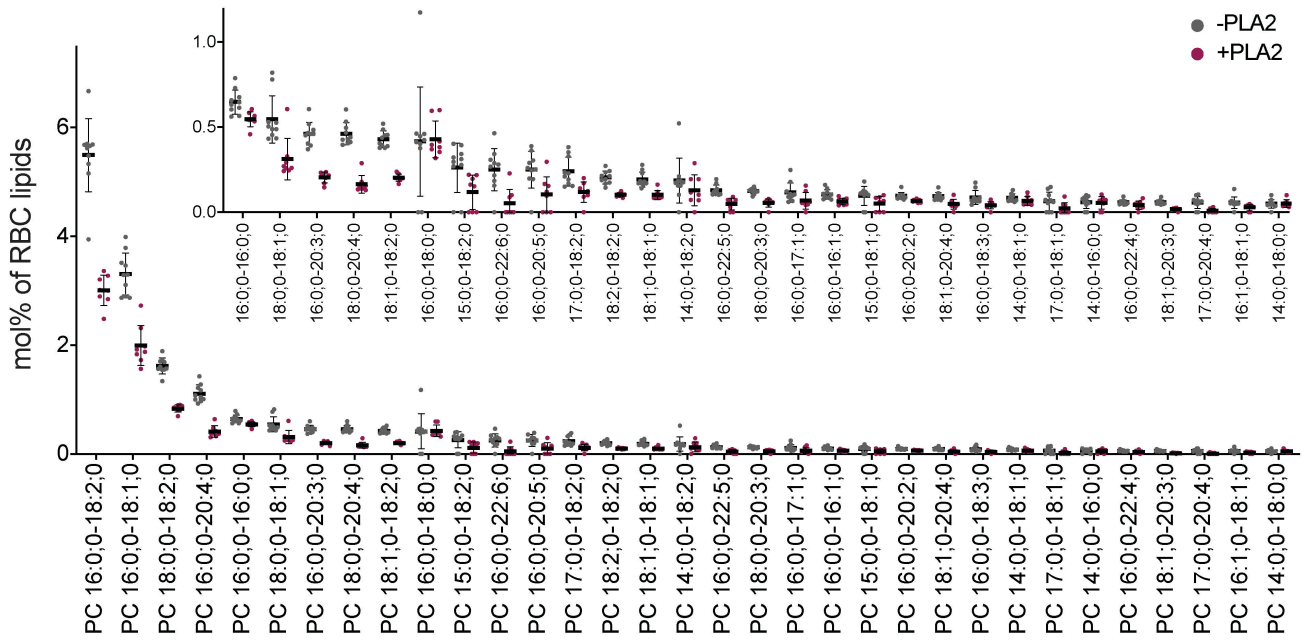

Supplementary Figure 2 – Variance in the lipidomic data. Shown are the individual data points and average ± SD of n>8 individual MS analyses from n=8-10 human donors. All species of PC above 0.05 mol% are shown for both untreated and PLA2-treated samples. Inset shows the more minor species with an expanded y-axis range.

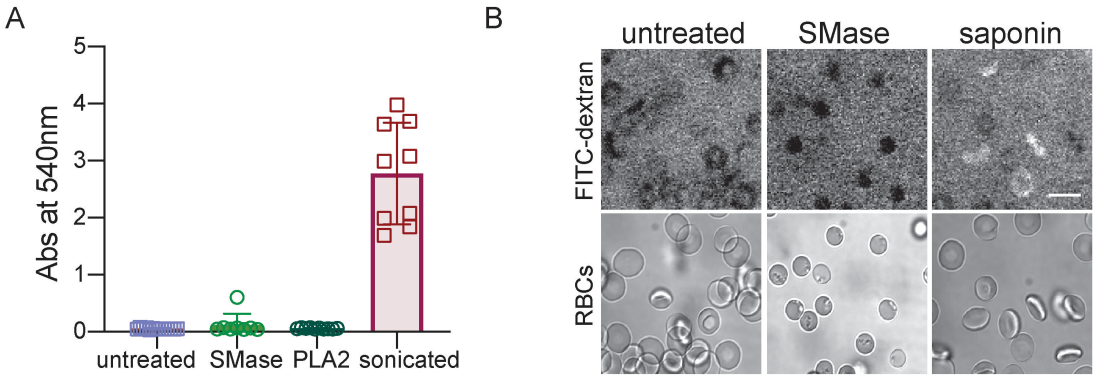

Supplementary Figure 3 – Lack of RBC hemolysis following SMase or PLA2 treatments. (A) Absorbance of supernatant at 540 nm after pelleting RBCs. Neither SMase nor PLA2 treatments lead to any observable absorbance above untreated RBCs, suggesting no leakage of hemoglobin, thus intact erythrocytes. Leakage of hemoglobin following sonication serves as the positive control. Individual data points and mean ± SD from 8-10 independent experiments are shown. (B) Both untreated and SMase-treated RBCs remain impermeable to FITC-dextran (visible by bright background fluorescence and dark cell interior), while saponin-permeabilized cells are completely penetrated, as evidenced by approximately equal FITC-dextran signal inside the cells as outside. These results illustrate that SMase-treated RBCs remain intact and impermeable. Top row shows FITC-dextran fluorescence; bottom row shows pseudo-DIC image to visualize cells. Scale bar is 10 μm.

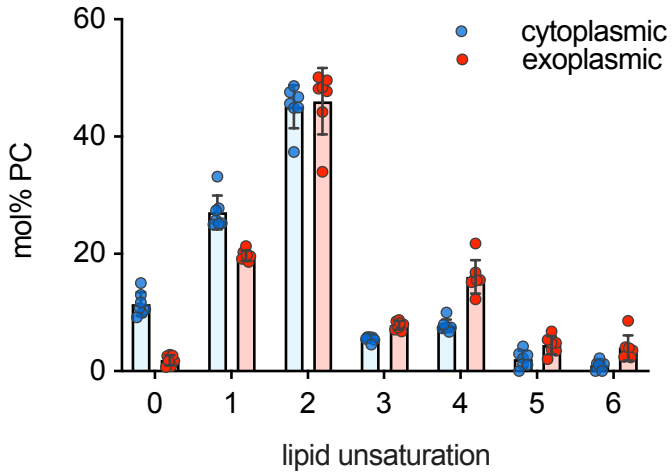

Supplementary Figure 4 – Asymmetry of phosphatidylcholine acyl chain unsaturation. PC tends to be more unsaturated in the exoplasmic leaflet of the RBC membranes. Fully saturated acyl chains are highly enriched in the cytoplasmic leaflet while exoplasmic leaflets contain more polyunsaturated chains. Individual data points and mean ± SD from 7 independent experiments are shown.

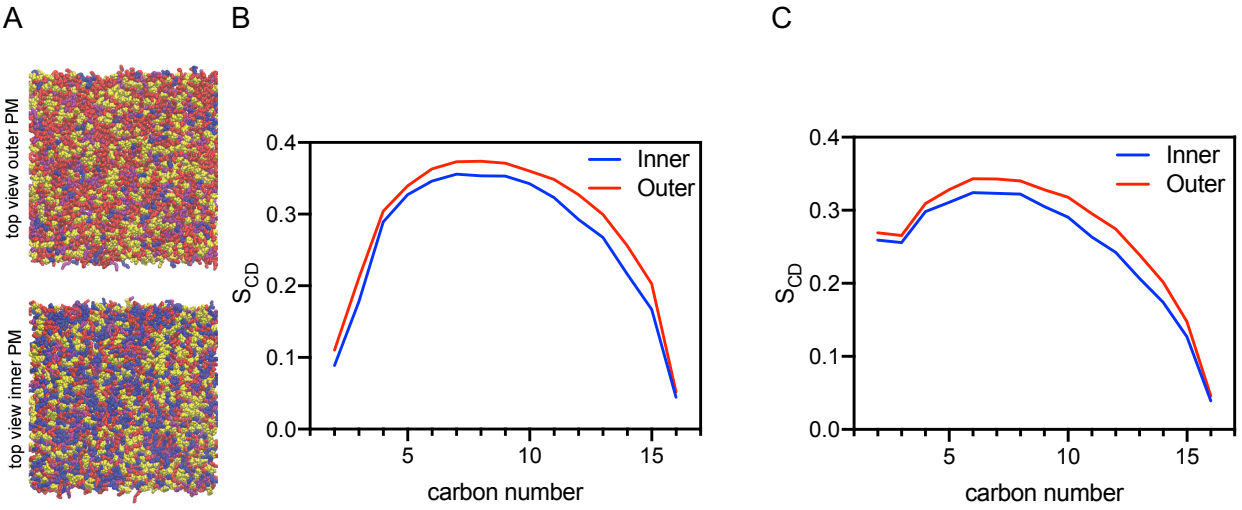

Supplementary Figure 5 – Atomistic simulation of biophysical asymmetry of erythrocytes PM. (A) Final snapshots of outer- and inner-PM leaflet mimetic simulations (yellow = cholesterol, red = saturated acyl chains, purple = mono- and di-unsaturated, blue = polyunsaturated; headgroups not shown in top views). (B-C) Computed deuterium order parameters (S_{CD}) of lipids in inner versus outer PM simulations - (B) the fatty acyl chain of palmitoyl sphingomyelin (PSM) and (C) the sn-1 chain of 1-palmitoyl-2-linoleoyl PC (16:0/18:2 PC).

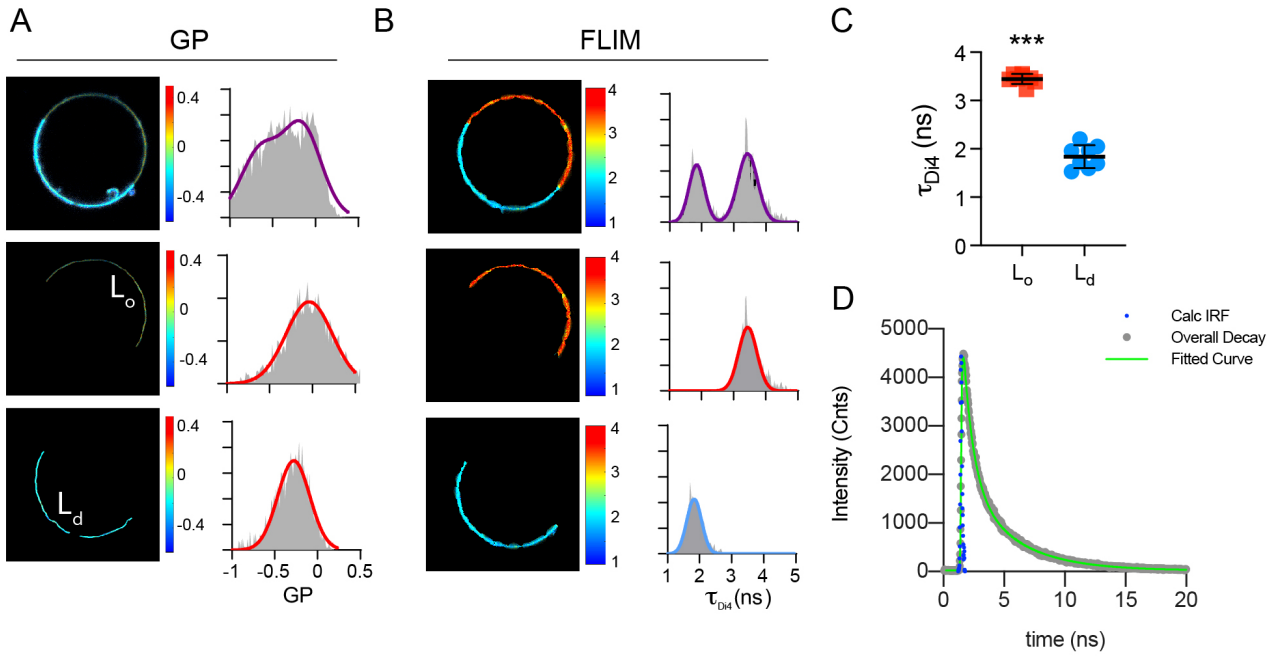

Supplementary Figure 6 – Characterization of Di4 for measuring lipid packing differences. (A) Average GP and lifetime images of Di4 in a phase separated GUV composed of DOPC/DPPC/Cholesterol (40:40:20). The intensity-weighted average lifetime and GP histograms were fit with either a double (whole GUV, GPMV violet line) or single (L_o or L_d phase, red and blue line) Gaussian, respectively. (C) Average lifetime of Di4 in L_o and L_d in GUVs. Individual data points and mean ± SD from 8 independent experiments are shown. $p<0.001$ computed from unpaired, two-tailed t-test. (D) Representative lifetime curve of Di4 from outer leaflet-stained RBL cells showing the instrument response function (IRF), overall decay data points, and the two-component regression fit ($\tau_{Di4} = 3.15$ ns).

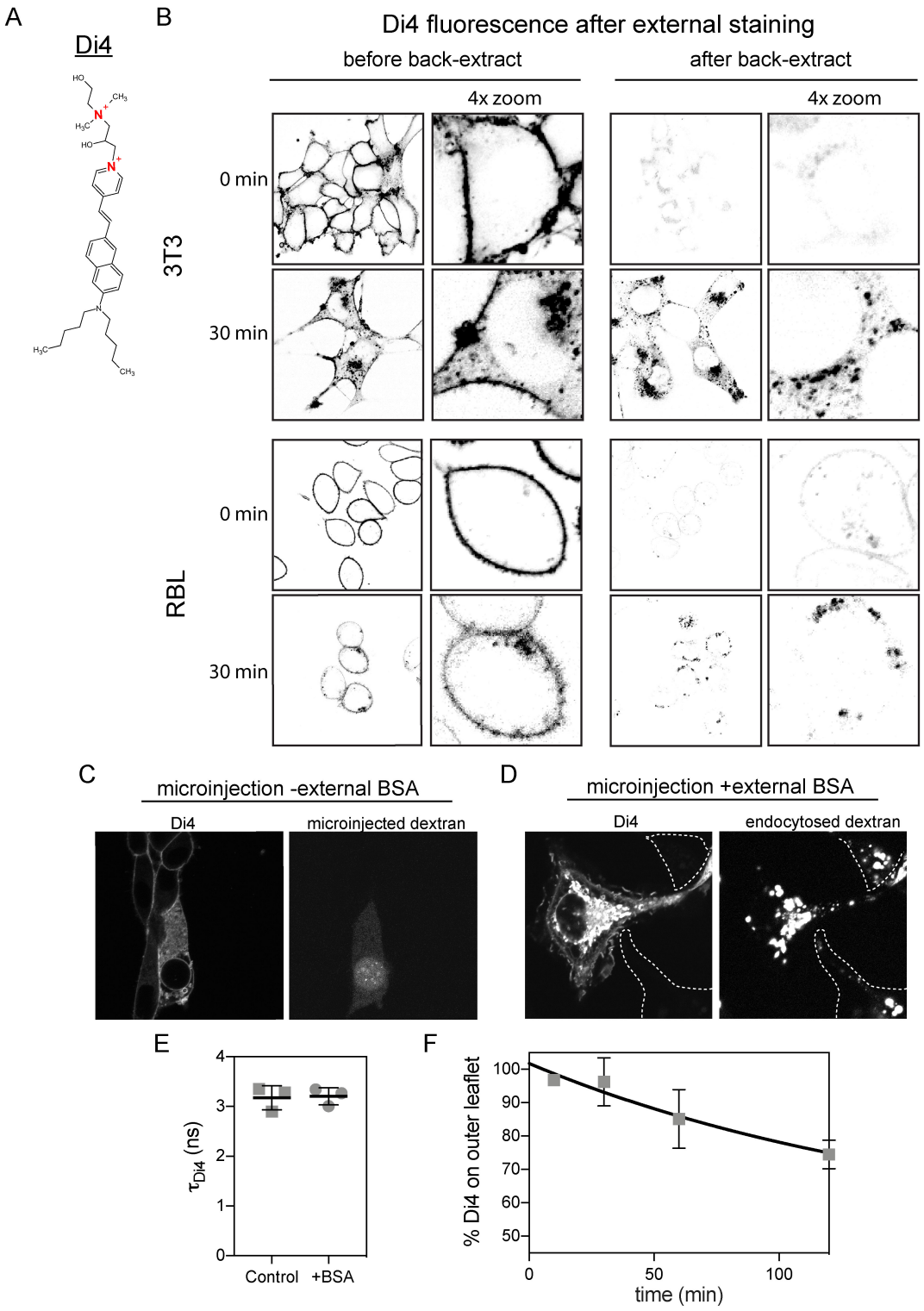

Supplementary Figure 7 – Characterization of leaflet selective PM staining by Di4. (A) di-4ANEPPDHQ (Di4) chemical structure containing 2 positively charged quarternary ammonium groups (red). (B, left) External staining of cells at the PM after staining with Di4. Time 0 is imaging immediately after Di4 incubation and wash. The bottom panels in each group show cells after 30 min incubation at 37°C to allow dye internalization into endosomes. (B, right) Addition of BSA leads to near complete extraction of Di4 suggesting it is solely in the exoplasmic PM leaflet at time 0. After dye is endocytosed (30 min incubation at 37°C), it is not extractable by BSA; however, the dye remaining on the PM is completely extracted. This observation suggests minimal flipping across the bilayer on our experimental time scale. (C) Microinjection of Di4 in the absence of external BSA leads to staining of both the microinjected cell (visualized by co-microinjected dextran-cascade blue at 4 mg/ml) and surrounding cells due to leakage of dye from micropipette. (D) Inclusion of BSA into the bathing media eliminates off-target staining (other cells in the field visualized by endocytosed fluorescent dextran). There remains robust staining of the PM in the target cell because the dye is on the inner leaflet which is not accessible to BSA back-extraction. The same effect (i.e. no extraction of internal membranes by BSA after microinjection) was observed after incubating the cells for up to 60 min at 37°C. (E) BSA treatment itself had no effect on the properties of the PMs. For this experiment, RBLs were incubated with 1.5% BSA at 4°C (3 times for 10 mins), washed with PBS, the *subsequently* stained with Di4 as described in the Materials and

Methods. The lifetime of Di4 on the PM was not affected by 'pre-treatment' with BSA, suggesting that BSA itself does not have an effect on membrane properties. (F) To determine the intrinsic flipping rate of Di4 under controlled conditions, we constructed symmetric liposomes (large unilamellar vesicles; LUVs) containing Di4. We then incubated the LUVs with potassium iodide (KI) to quench the fluorescence of externally accessible Di4 (see Methods). Probe flipping results in reduction of quenching efficiency, because KI cannot cross the membrane. Although some flipping was observed, the magnitude was minimal through the time course of the experiment. Fitting to first-order kinetics suggested a flipping rate of (k_{flip}=0.0056 min^{-1}, $C.I._{(95\%)}$ = 0.0039-0.0075 min^{-1}) with resulting time constant for loss of asymmetry being ~164 min. Thus, on the maximal time-scale of our experiments (60 min), ~14% of the probe would be expected to flip between leaflets, which would only slightly influence the measurements of overall leaflet order. Moreover, we point out that these experiments were done in cholesterol-free liposomes, while the cholesterol-rich PM would be expected to be even less amenable to flip-flop. (E-F) Mean ± SD from 3 independent experiments.

Disparities in biophysical properties between the two leaflets of the PM in living cells have long been proposed but remain ambiguous due to experimental limitations and inconsistencies. For example, EPR studies found that spin-labeled phosphatidylcholine (PC) was found in a more rigid environment than amine-headgroup lipids, implying that the inner leaflet of the PM is more fluid [1,2]. In opposition, several studies with various fluorescent probes reported a more fluid outer leaflet [3-7]. Similar inconsistencies have been reported by measurements of diffusion with NBD-labeled lipids, with some inferring slower diffusion of outer leaflet components [8,9], while others reported faster diffusion in the outer leaflet at low temperatures and minimal differences at physiological temperature [10]. Similarly, NBD-labeled phosphoinositides diffused faster in the outer leaflet compared to the inner [11]. Most recently, lifetime of NBD-labeled lipids suggested that the outer leaflet is more tightly packed [12].

Despite these significant investigations, the presence and nature of biophysical asymmetry in mammalian membranes has remained unresolved because of several limitations inherent to methodologies that rely on probes based on biological lipids and/or fluorescence quenchers: (1) fluorescence quenchers are toxic and potentially membrane disruptive. Further, their membrane impermeability is questionable and is rarely tested. (2) The localization of the probe in the cell is often not directly known or reported; PM localization has been often assumed but not usually directly imaged. (3) Limited direct knowledge of probe asymmetry. (4) Possible interactions between probes and other lipids, proteins and the cytoskeleton. (5) Interconversion or degradation of fluorescent lipid analogs [13]. In contrast, the probes used here (Di4 and NR12S) are intended to be biologically inert, in that they are not expected to be metabolized like native lipids or to be toxic or disruptive. Direct imaging confirms that they remain on the PM, where their flipping rate can be directly quantified.

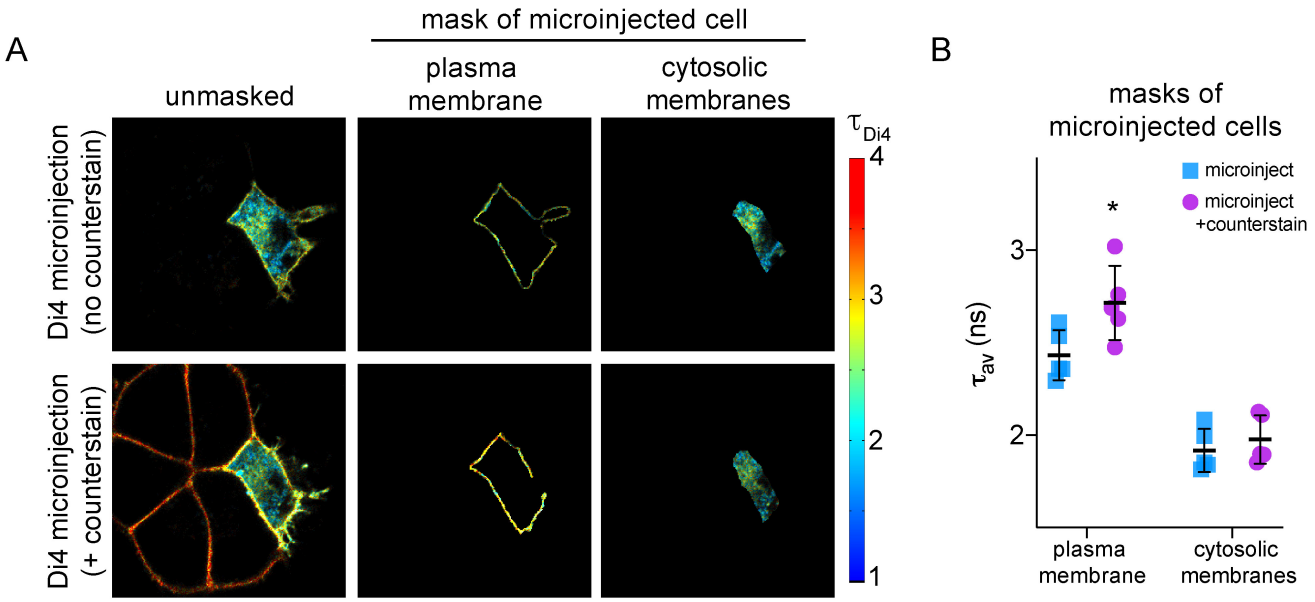

Supplementary Figure 8 – Leaflet selective lifetime of Di4. (A, top row) A single RBL cell was microinjected with Di4 in the presence of external BSA and imaged via FLIM. Without BSA in the medium, surrounding cells are always stained by Di4 leaking out of the microinjection pipette (e.g. see Fig S6C). However, inclusion of BSA leads to Di4 extraction from the outer leaflet, such that only the microinjected cell is visible. (A, bottom row) After imaging and washing away the external BSA, the same cells were re-incubated with Di4 and imaged. Shown are Di4 FLIM images, with PM (middle) and cytosolic membrane (right) masks of the microinjected cell. In the bottom row (after external labeling), the microinjected cell has Di4 in both PM leaflets, whereas the surrounding cells are only stained on the external leaflet, as revealed by the distinct Di4 lifetimes in the PMs. (B) Di4 lifetime of the PM and cytoplasmic membranes of microinjected cells before and after external staining with Di4. Di4 lifetime on the PM is increased by

external staining, due to signal coming from both the internal and external PM leaflets. On the other hand, the lifetime of the internal membranes is unaffected. Individual data points and mean ± SD are shown.

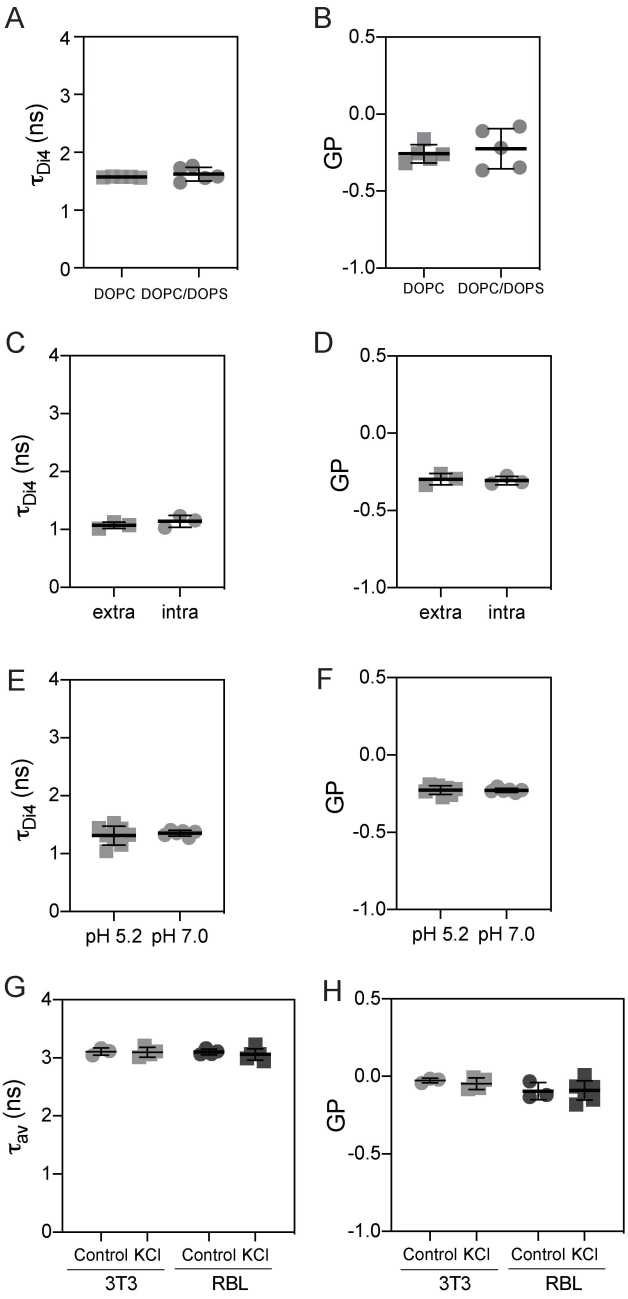

Supplementary Figure 9 – Control experiments to exclude the possibility that Di4 is sensing differences in leaflet charge density, ion composition, pH, or membrane potential. (A) FLIM and (B) GP imaging of Di4 in GUVs composed of either pure DOPC or DOPC with 20% charged lipid (DOPC/DOPS ; 4:1). (C) FLIM and (D) GP of Di4 in GUVs composed of DOPC and incubated in extra- or intracellular buffer. (E) FLIM and (F) GP of Di4 in GUVs composed of DOPC and incubated in 20mM HEPES, pH 5.2 or pH 7.0. Neither lifetime nor GP was affected by the negatively charged DOPS, pH, or ionic strength/composition of buffer suggesting no effect of charged lipids or relevant environmental conditions on Di4 photophysical properties. (G) FLIM and (H) GP imaging of Di4 stained cells before and after membrane depolarization with 100 mM KCl. We observed no effect of membrane depolarization on either parameter, confirming previous observations that membrane potential does not significantly affect Di4 emission spectra [14]. Finally, Di4 fluorescent properties are insensitive to protein content of the membrane [15], excluding asymmetric protein density as the explanation for our observations. Individual data points and mean ± SD are shown.

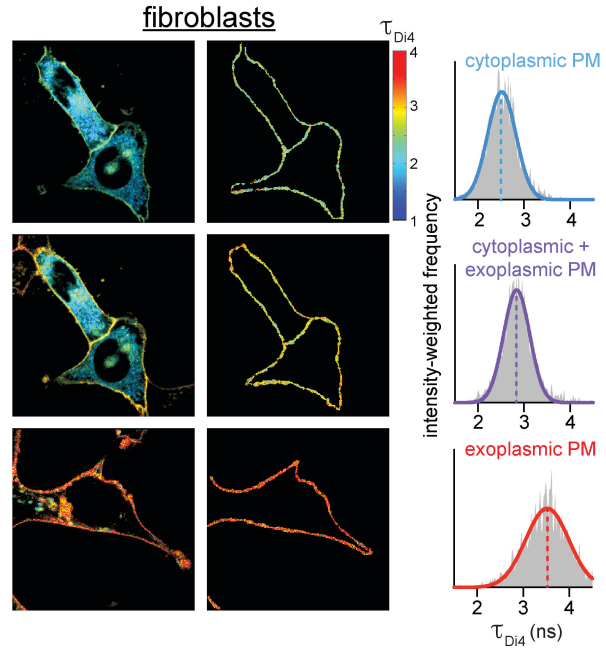

Supplementary Figure 10 – Di4 GP imaging confirms the order differences between inner and outer plasma membrane leaflets. Exemplary GP images of (A) mast cells or (B) 3T3 fibroblasts showing (left) whole cells, (middle) PM masks and, (right) intensity-weighted histograms of the PM mask in cytosolic leaflets (microinjected), both leaflets (outside stain+microinjected), and outer leaflet (outside stain). (C) Average GP of plasma membrane masks of microinjected (blue) vs. outer leaflet stain (red) in both cell types.

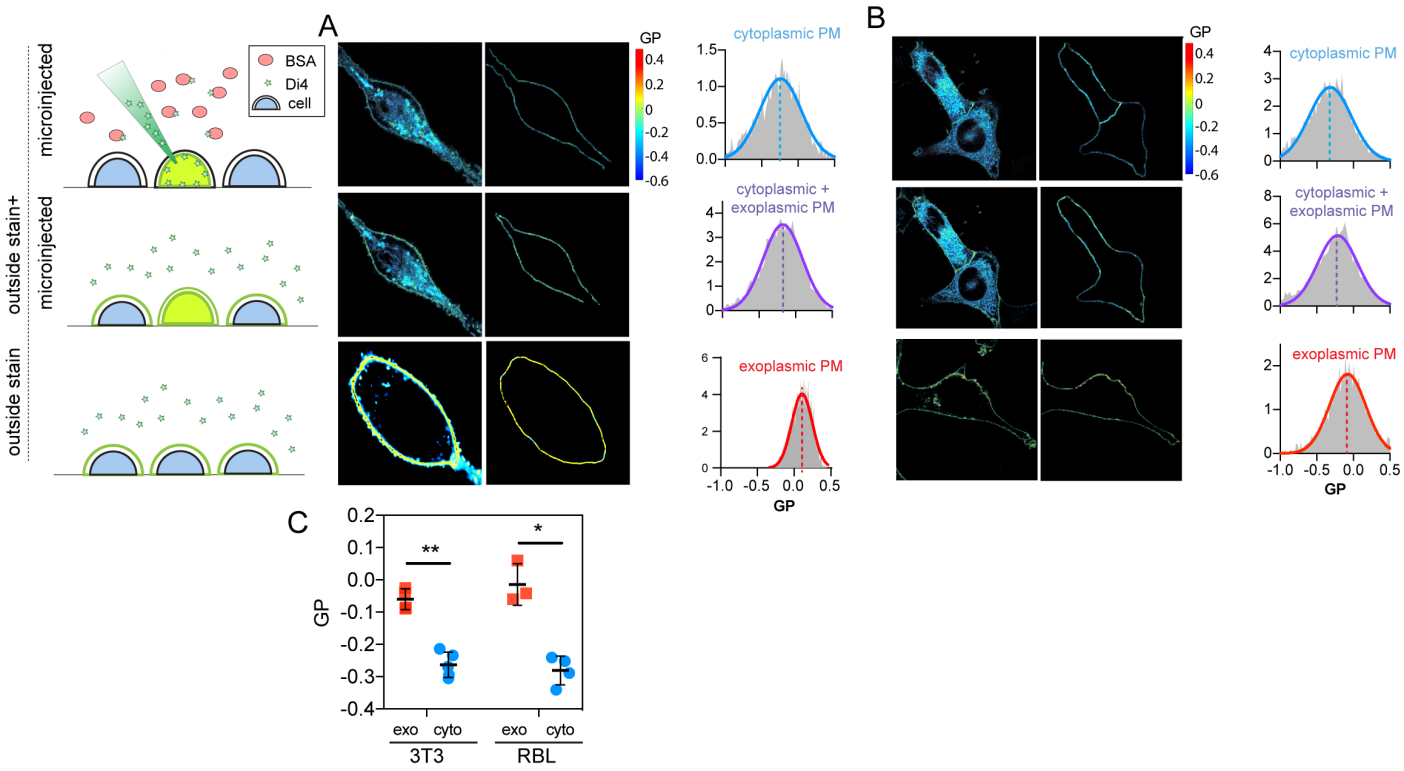

Supplementary Figure 11 – Di4 GP imaging confirms the order differences between inner and outer plasma membrane leaflets. Exemplary GP images of (A) mast cells or (B) 3T3 fibroblasts showing (left) whole cells, (middle) PM masks and, (right) intensity-weighted histograms of the PM mask in cytosolic leaflets (microinjected), both leaflets (outside stain+microinjected), and outer leaflet (outside stain). (C) Average GP of plasma membrane masks of microinjected (blue) vs. outer leaflet stain (red) in both cell types. Individual data points and mean ± SD are shown. ***p<0.001 using Sidak's multiple comparison test.

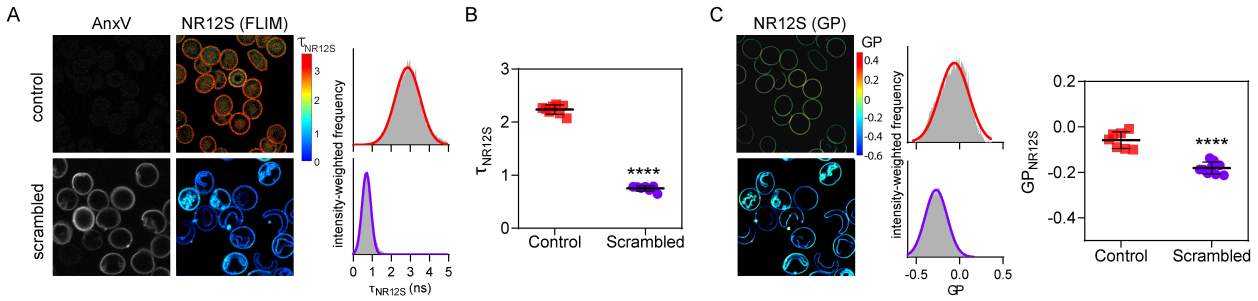

Supplementary Figure 12 – Confirmation of reduction of lipid packing in scrambled vs. unscrambled RBCs probed by leaflet selective, order sensitive dye NR12S. (A) AnxV staining, (B) FLIM, and (C) GP imaging of NR12S in untreated (control) vs. PMA (10 μM, scrambled) RBCs. Treatment with PMA induces membrane scrambling, as evidenced by wholesale PS exposure. This scrambling leads to dramatic reduction of NR12S lifetime (A-B) and GP (C), suggesting that the outer leaflet of the RBC PM becomes much less packed. These observations suggest that the inner leaflet is much less packed than the outer in resting RBCs. Importantly, AnxV was added right after FLIM or GP-imaging of Di4 to confirm the loss of asymmetry in the imaged cells but avoid any interference with Di4 or NR12S emission. Individual data points and mean ± SD are shown. ***p<0.001 using unpaired two-tailed t-test.

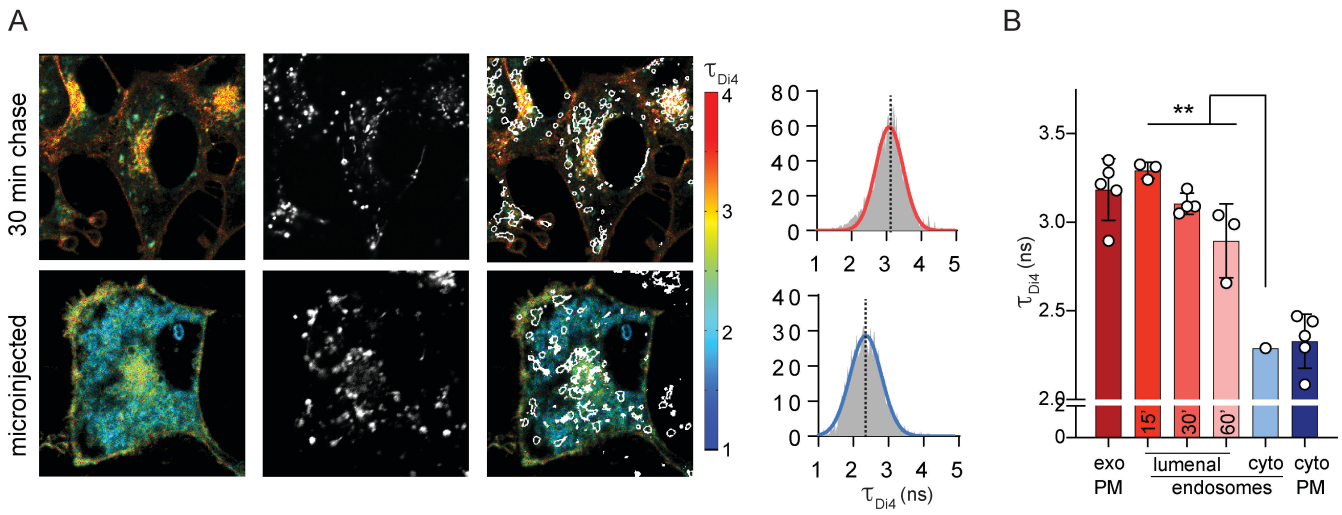

Supplementary Figure 13 – Endosome asymmetry in 3T3 fibroblasts. (A) Exemplary FLIM images of Di4 lifetime and dextran fluorescence following a two-hour incubation with fluorescent dextran, 10-minute staining with Di4, then a 30-minute incubation without either label to "chase" dyes into endosomes. The localization of dextran (middle) is used to create an endosomal membrane mask (right images) to derive intensity-weighted histograms of τ_{Di4} (right). (B) The high lifetime (i.e. lipid packing) of the exoplasmic PM leaflet is maintained up to 60 min after endocytosis.

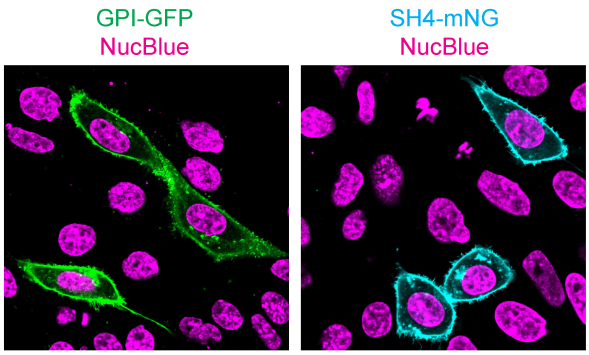

Supplementary Figure 14 – GPI-GFP and SH4-mNG localize to the plasma membrane.

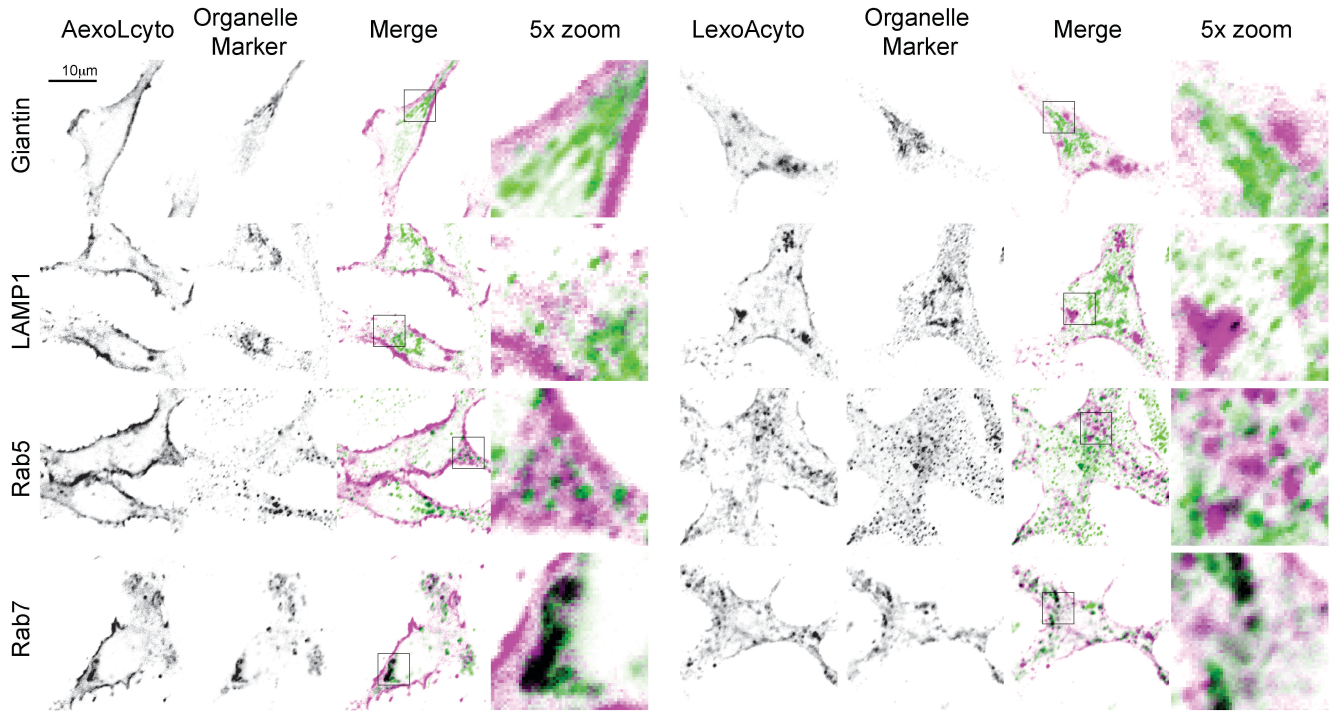

Supplementary Figure 15 – Subcellular localization of AexoLcyto-RFP and LexoAcyto-RFP. RBL cells were transfected with the indicated plasmid, fixed after 24 hr, and immunofluorescence performed. Images were acquired at 100x on a Nikon A1R confocal microscope.

1 Tanaka, K. I. & Ohnishi, S. Heterogeneity in the fluidity of intact erythrocyte membrane and its homogenization upon hemolysis. *Biochim Biophys Acta* **426**, 218-231 (1976).

2 Seigneuret, M., Zachowski, A., Hermann, A. & Devaux, P. F. Asymmetric lipid fluidity in human erythrocyte membrane: new spin-label evidence. *Biochemistry* **23**, 4271-4275 (1984).

3 Cogan, U. & Schachter, D. Asymmetry of lipid dynamics in human erythrocyte membranes studied with impermeant fluorophores. *Biochemistry* **20**, 6396-6403 (1981).

4 Schroeder, F. Differences in fluidity between bilayer halves of tumour cell plasma membranes. *Nature* **276**, 528-530 (1978).

5 Igbavboa, U., Avdulov, N. A., Schroeder, F. & Wood, W. G. Increasing age alters transbilayer fluidity and cholesterol asymmetry in synaptic plasma membranes of mice. *Journal of neurochemistry* **66**, 1717-1725 (1996).

6 Schachter, D., Abbott, R. E., Cogan, U. & Flamm, M. Lipid fluidity of the individual hemileaflets of human erythrocyte membranes. *Annals of the New York Academy of Sciences* **414**, 19-28 (1983).

7 Nikolova-Karakashian, M. N., Petkova, H. & Koumanov, K. S. Influence of cholesterol on sphingomyelin metabolism and hemileaflet fluidity of rat liver plasma membranes. *Biochimie* **74**, 153-159 (1992).

8 Morrot, G. *et al.* Asymmetric lateral mobility of phospholipids in the human erythrocyte membrane. *Proc Natl Acad Sci U S A* **83**, 6863-6867 (1986).

9 el Hage Chahine, J. M., Cribier, S. & Devaux, P. F. Phospholipid transmembrane domains and lateral diffusion in fibroblasts. *Proc Natl Acad Sci U S A* **90**, 447-451 (1993).

10 Rimon, G., Meyerstein, N. & Henis, Y. I. Lateral mobility of phospholipids in the external and internal leaflets of normal and hereditary spherocytic human erythrocytes. *Biochim Biophys Acta* **775**, 283-290 (1984).

11 Golebiewska, U., Nyako, M., Woturski, W., Zaitseva, I. & McLaughlin, S. Diffusion coefficient of fluorescent phosphatidylinositol 4,5-bisphosphate in the plasma membrane of cells. *Mol Biol Cell* **19**, 1663-1669, doi:10.1091/mbc.E07-12-1208 (2008).

12 Gupta, A., Korte, T., Herrmann, A. & Wohland, T. Plasma membrane asymmetry of lipid organization: fluorescence lifetime microscopy and correlation spectroscopy analysis. *J Lipid Res* **61**, 252-266, doi:10.1194/jlr.D119000364 (2020).

13 Lipsky, N. G. & Pagano, R. E. Sphingolipid metabolism in cultured fibroblasts: microscopic and biochemical studies employing a fluorescent ceramide analogue. *Proc Natl Acad Sci U S A* **80**, 2608-2612 (1983).

14 Wang, Y., Jing, G., Perry, S., Bartoli, F. & Tatic-Lucic, S. Spectral characterization of the voltage-sensitive dye di-4-ANEPPDHQ applied to probing live primary and immortalized neurons. *Optics express* **17**, 984-990 (2009).

15 Dinic, J., Biverstahl, H., Maler, L. & Parmryd, I. Laurdan and di-4-ANEPPDHQ do not respond to membrane-inserted peptides and are good probes for lipid packing. *Biochim Biophys Acta* **1808**, 298-306, doi:10.1016/j.bbamem.2010.10.002 (2011).